Error Correction Code for FSCM-based Acoustic Underwater Communication

Julia Marie Wüpperling[1], Fabian Steinmetz[1], and Bernd-Christian Renner[1]

[1]Hamburg University of Technology, Institute for Autonomous Cyber-Physical Systems

Bernd-Christian Renner
Hamburg University of Technology
Institute for Autonomous Cyber-Physical Systems
Harburger Schloßstraße 28, 21079 Hamburg, Germany
christian.renner@tuhh.de

Abstract: *Efficient and reliable low-power acoustic underwater communication is essential for underwater applications, such as wireless sensor networks or swarms of miniature underwater robots. Moreover, underwater communication is already part of 6G. Our recent research focused on frequency shift chirp modulation (FSCM), which is already used for low-power overwater radio communication. However, the acoustic underwater channel differs in terms of propagation speed, Doppler shifts, attenuation, and multipath propagation. While we have already implemented the de-/modulation, in this paper we look into identifying an appropriate error correction code. First, we analyze the error distribution of our current FSCM implementation to understand the underlying causes of errors and their patterns. Second, we evaluate different error correction codes for FSCM through simulations in Watermark using real-world channel impulse responses. Our research demonstrates significant improvements in reliability for underwater communication, contributing to the underwater research community's pursuit of developing new solutions for low-power underwater applications.*

Keywords: *underwater communication, acoustic, FSCM, chirp, coding*

1. INTRODUCTION

Underwater Acoustic Communication (UWAC) systems are integral to various marine applications; e.g., the deployment of Underwater Wireless Sensor Networks (UWSNs) for environmental monitoring and scientific research. UWSNs may consist of a variety of sensor nodes, such as stationary seafloor units, surface buoys, Autonomous Underwater Vehicles (AUVs), and Autonomous Surface Vehicles (ASVs). These nodes collaboratively collect mission-specific data, ranging from seafloor pressure for tsunami detection to water quality parameters for monitoring marine ecosystem health [4]. To enable long-term autonomous operation, they may be equipped with low-power components and operate with limited computational resources [11].

Reliable communication is fundamental for successful data collection and remote control. However, utilizing underwater acoustic channels for signal transmission poses unique challenges, since phenomena such as absorption, multipath propagation, Doppler effects and environmental noise can significantly impair signal quality [6]. Especially in low-power systems, energy-efficient communication and avoidance of retransmissions is mandatory.

As we recently demonstrated in [12], the relatively new modulation technique Frequency Shift Chirp Modulation (FSCM), developed in the context of low-power radio communication, offers strong resilience against these impairments compared to traditional modulation schemes such as Frequency Shift Keying (FSK). To mitigate remaining transmission errors, channel coding is required for forward error correction [8]. Unitl now, channel coding for (underwater acoustic) FSCM has received little attention in existing research.

We address this gap by investigating the integration of FSCM with channel coding strategies suitable for low-power UWAC systems through the following contributions:

- **Analysis of Uncoded FSCM Transmissions:** In a simulation study in Section 3, we analyze how errors manifest in FSCM transmissions without channel coding. We study bit errors and packet reception success under various channel conditions.
- **Evaluation of Coded FSCM Transmissions:** In Section 4, we extend the previous study with coded FSCM. To assess the trade-off between reliability and transmission efficiency, improvements in packet reception are quantified alongside the impact on the data rate.
- **Recommendation of Practical Channel Codes:** Based on a final discussion in Section 4, we give recommendations for channel coding strategies in FSCM-based low-power UWAC systems.

2. RELATED WORK

In the last decade, LoRaWAN [5] was developed and implemented for over-water Low-Power Wide-Area Networks (LPWANs) such as Internet of Things (IoT) applications. LoRaWAN is composed of a physical (PHY) layer, the LoRa-PHY (frequently called LoRa), and a Medium Access Control (MAC) layer. The LoRa-PHY uses Chirp Spread Spectrum (CSS) modulation, which is usually called FSCM [18]. However, the LoRa-PHY is a proprietary standard, and implementation details are unspecified. Therefore, research has been conducted on packet synchronization and demodulation [16, 19], multipath propagation [3], error coding [1, 20], and real-world trials [5]. In general, FSCM showed remarkable resilience against multipath propagation and low Signal-to-Noise Ratios (SNRs) for over-water communication.

Motivated by the promising results from the over-water communication, researchers started to investigate FSCM for acoustic underwater communication [10, 7, 21]. However, the acoustic underwater channel differs from the over-water radio communication channel: The available bandwidth is smaller, the Doppler shifts are larger, and the acoustic channel is distorted by massive multipath propagation [15].

In previous publications, we showed resilience against multipath propagation [12] and developed methods to reduce the effect of Doppler shifts [13]. In real-world trials, we showed that our FSCM implementation for acoustic underwater communication achieves very low Bit Error Rates (BERs) [14]. However, we observed a difference between the static and mobile transmission channels. Our Doppler shift removal reduces the BERs, but the BER was higher compared to static scenarios. Until now, we have not applied any error correction codes to detect and correct transmission errors. Likewise, other researchers have also implemented FSCM without additional error coding [10, 7, 21]. Therefore, error correction codes for FSCM-based acoustic underwater communication are a prevailing research gap.

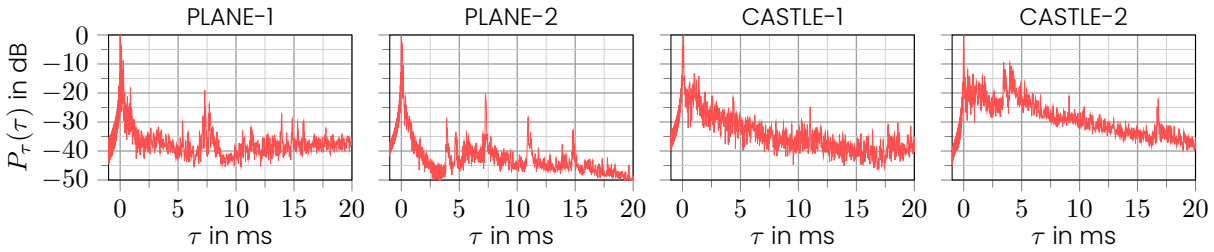

Figure 1: Power delay profiles of real-world acoustic underwater channels ($50\,\text{kHz} - 75\,\text{kHz}$*) from [12]. PLANE-1 and CASTLE-2 are used for the simulations.*

In over-water communication, on the contrary, FSCM has already been used with different codings. For example, LoRa uses a Hamming code [5]. Moreover, different codings have been investigated, for example, Hamming code [1], Reed-Solomon (RS) codes [2], and Low Density Parity Check (LDPC) codes [20]. We use this is a starting point for this paper.

3. ANALYSIS OF UNCODED FSCM TRANSMISSIONS

For selecting a favorable error coding and understanding the error characteristics of uncoded FSCM transmissions, we conducted a simulation study across diverse channel conditions.

3.1. SIMULATION SETUP AND METRICS

We ran simulations in MATLAB with our previously implemented differential FSCM modulation and demodulator [13]. To simulate the acoustic underwater channel, we use Watermark [17] with recorded channel impulse responses and apply configurable variations such as timing offsets, Doppler shifts, and noise levels. We compare demodulated output to the original data input and study the amount and distribution of bit errors. We transmit data packets with $128\,\text{B}$ of random data, modulated with spreading factors $\text{SF} \in \{6, 8, 10\}$. While a higher SF for the synchronization vs. data is favorable [14], we apply a common SF across the entire packet to limit the complexity. We use a subset of channel impulse responses from [12] shown in Fig. 1: PLANE-1 and CASTLE-2. They present challenging yet different conditions, where PLANE channels exhibit a dominant early-arriving path, followed by multiple closely spaced multipath components with gradually decreasing power. The CASTLE environments show denser and more prolonged multipath components, representing more complex conditions typically found in ports with multiple reflecting surfaces.

For each configuration, we evaluated 90 packets. The corresponding simulated acoustic signals are systematically modified to emulate realistic transmission impairments. Signal arrival times are varied within a range of $10\,\text{ms}$ to $100\,\text{ms}$ to simulate various propagation delays. Doppler shifts are introduced for relative velocities between $-3\,\text{m}\,\text{s}^{-1}$ and $3\,\text{m}\,\text{s}^{-1}$. We use SNR levels from $-6\,\text{dB}$ to $15\,\text{dB}$. Communication parameters—i.e., frequency band, sampling rate—match our ahoi modem [9]. Table 1 summarizes all simulation parameters.

Finally, the modified received signals are demodulated and compared to the original data input, which enables the direct assessment of the error characteristics of uncoded FSCM transmissions across the defined parameter space. We use Packet Success Rate (PSR)—the fraction of error-free packets—and BER—the fraction of erroneous bits—of all successfully synchronized packet transmissions per configuration for our evaluation. To assess the influence of packet length, we look into the first $8\,\text{B}$ of these packets separately.

Parameter	Symbol	Unit	Values
Packet size	n_{data}	B	128
Spreading Factor	SF	—	$6, 8, 10$
Bandwidth	BW	kHz	20
Carrier frequency	f_{c}	kHz	62.5
Sampling frequency	$f_{\text{s,tb}}$	kHz	200
Channel	—	—	PLANE-1, CASTLE-2
Number of evaluated packets	n_{pkt}	—	90
Time delay	δ_{t}	ms	$10 - 100$
Relative speed	v	$\text{m}\,\text{s}^{-1}$	$-3, -1.5, 0, 1.5, 3$
Signal-to-noise ratio	SNR	dB	$-6, -3, 0, 3, 6, 9, 12, 15$

Table 1: Simulation parameters for uncoded FSCM transmissions.

3.2. RESULTS

Figures 2 and 3 present the PSR and BER for $8\,\text{B}$ and $128\,\text{B}$ data packets in the PLANE-1 and CASTLE-2 channels, respectively. To indicate cases of error-free reception, the BER plots include a *BER resolution* line, indicating the smallest non-zero BER for the packet length. It is 1.74×10^{-4} for $8\,\text{B}$ packets and 1.09×10^{-5} for $128\,\text{B}$ packets. For configurations without any synchronized packets—thus, no packet was demodulated—the BER and PSR are set to 0.5 and 0, respectively. This only occured in few configurations for $\text{SF} = 6$ and a negative SNR.

Variations of PSR and BER values for adjacent SNR levels stem from the small number of transmitted packets. As a result, even minor differences in the number of correctly demodulated packets can noticeably shift PSR values, and few additional bit errors near the BER resolution threshold are observed as visible steps in the BER curves.

The PSR and BER trends in PLANE-1 exhibit similiar patterns across both packet sizes in Figs. 2(a) to 2(b). For all values of SF, the PSR increases with higher SNRs, while the BER decreases accordingly. This aligns with the expectation that lower noise levels improve demodulation. Only the combination of $\text{SF} = 10$ with non-zero relative speeds deviates from this trend, where both metrics remain nearly constant across all SNR levels. This suggests that at $\text{SF} = 10$ demodulation is primarily limited by Doppler effects rather than noise. In fact, as v increases, the PSR reduces notably, falling below $5\,\%$ for $v = 3\,\text{m}\,\text{s}^{-1}$, while the BER remains high. This observation supports an increased sensitivity for $\text{SF} = 10$ to motion-induced frequency distortions. In contrast, $\text{SF} = 6$ and $\text{SF} = 8$ show greater resilience to Doppler shifts, with less diverging PSR and BER curves across different relative velocities.

Conversely to the Doppler effect, variations in packet length have a stronger influence at $\text{SF} = 6$ and $\text{SF} = 8$. This is evident from the lower PSR for long packets ($128\,\text{B}$). One cause of this behavior lies in Doppler estimation accuracy: lower spreading factors result in shorter symbol durations, reducing Doppler estimation precision. While short packets may still be demodulated correctly under small inaccuracies in the estimated time scaling, the misalignment between the receiver's sampling window and the actual symbol positions progressively increases with packet length, leading to lower PSR and higher BER values. The increased symbol duration of $\text{SF} = 10$, in contrast, allows for more accurate Doppler estimation, resulting in similar PSR and BER values across both packet lengths.

The trends in CASTLE-2 generally follow those observed in PLANE-1, but show notable differences across spreading factors and mobility. For $\text{SF} = 6$, the PSR is lower, particularly for longer packets, where it remains below $40\,\%$. This degradation can be attributed to stronger multipath interference. According to the channel's Power Delay Profile (PDP) (see

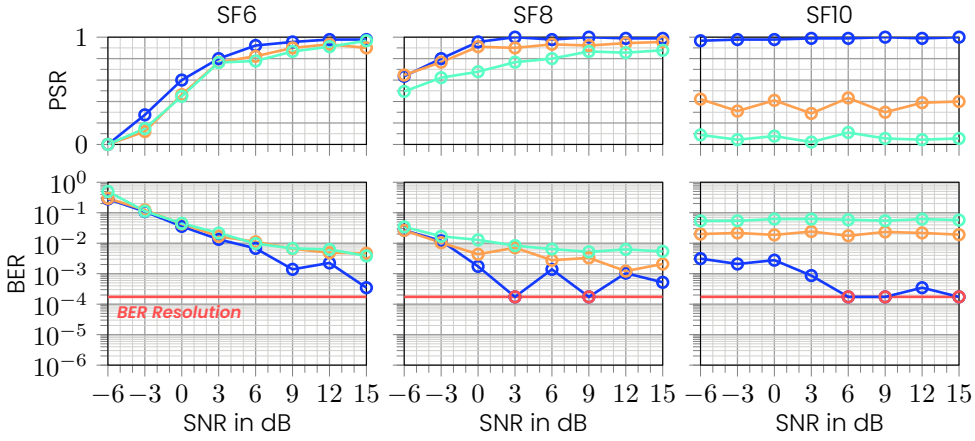

(a) PSR and BER for 8 B uncoded data.

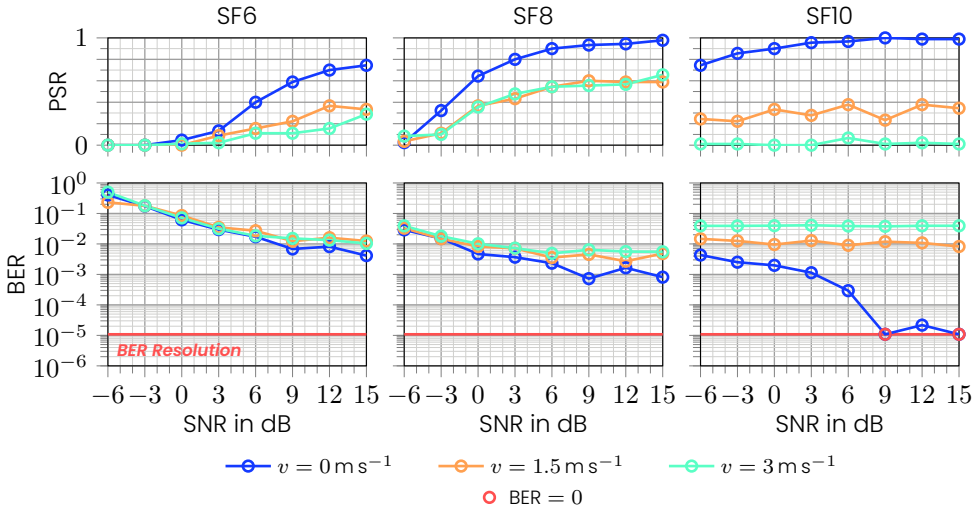

(b) PSR and BER for 128 B uncoded data.

Figure 2: PSR and BER of 8 B *and* 128 B *uncoded data in PLANE-1.*

Fig. 1), CASTLE-2 exhibits strong reflections around 3 ms to 4 ms after the main path. With a symbol duration of only 3.2 ms at SF $= 6$, these reflections overlap with subsequent symbols and degrade demodulation accuracy in terms of inter-symbol interference. For SF $= 8$, however, CASTLE-2 produces less errors, especially at higher SNRs. Additionally, Doppler-induced packet loss is reduced, as the PSR and BER in mobile scenarios converge towards the stationary case. This behavior may be attributed to CASTLE-2's stronger and more sustained multipath components within the 12.8 ms symbol duration of SF $= 8$, which produces less inter-symbol interference. A similar improvement is observed for SF $= 10$, where the PSR in mobile scenarios is approximately 10 % higher compared to PLANE-1. Notably, the observed improvements in PSR and BER over PLANE-1 are more pronounced for shorter packets, while longer packets still experience substantial packet loss.

3.3. SUMMARY

The results indicate that uncoded FSCM transmissions exhibit limitations under challenging transmission conditions; e.g., significant Doppler shifts or symbol lengths in the order of the channel delay spread. SF $= 10$ enables reliable demodulation in stationary scenarios even at low SNR. In contrast, SF $= 6$ and SF $= 8$ are more robust to Doppler shifts, maintaining

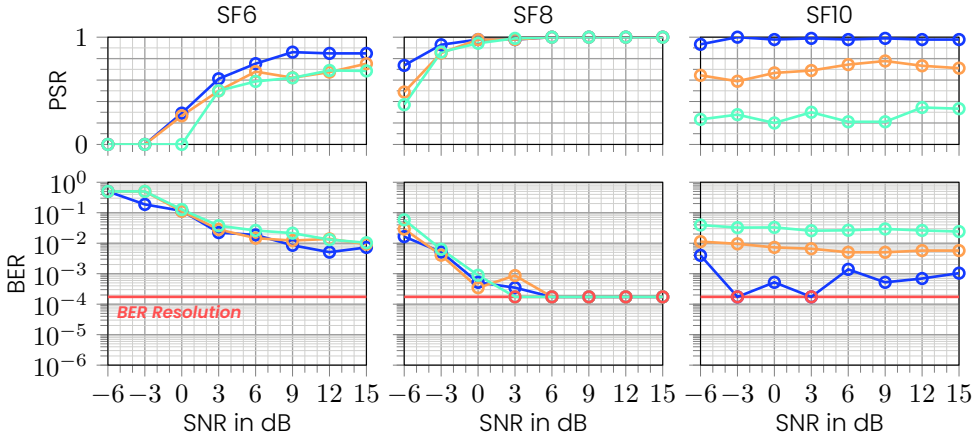

(a) PSR and BER for 8 B uncoded data.

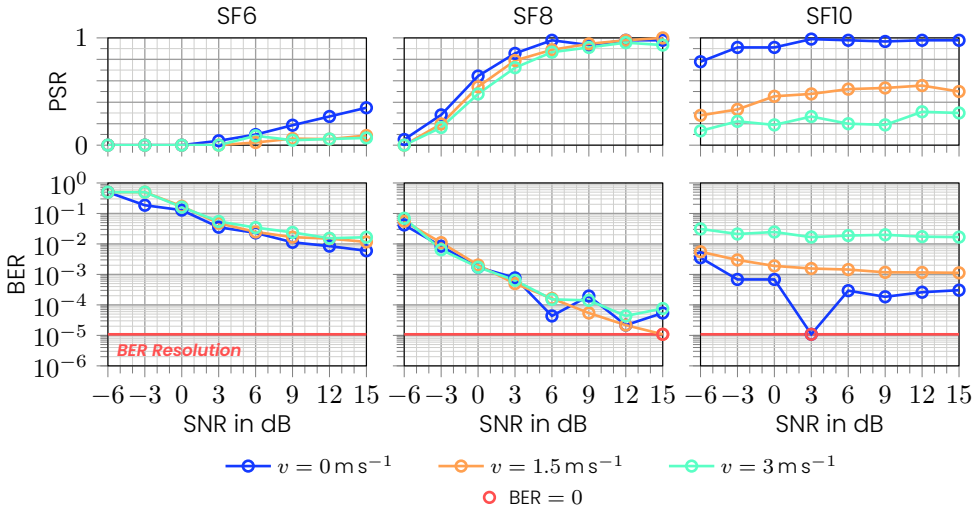

(b) PSR and BER for 128 B uncoded data.

Figure 3: PSR and BER of 8 B *and* 128 B *uncoded data in CASTLE-2.*

higher PSR values under motion. However, they require higher SNR levels to achieve reliable demodulation, with SF $= 6$ being particularly noise-sensitive.

Given these findings, channel coding is useful to improve communication reliability. Moreover, the results indicate that the BER has a high range across the parameters, and a considerable amount of packets can be transmitted without any bit error. We also found randomly distributed and burst bit errors in our study. Due to the page limitation, we omitted these results and the complex discussion.

4. EVALUATION OF CODED FSCM TRANSMISSIONS

To evaluate the effect of channel coding on FSCM-based low-power UWAC, we repeated the previous study with different coding techniques. We used available MATLAB functions. Based on the codes used in LoRa (cf. Section 2), the small packet sizes in acoustic underwater communication, and our results from Section 3, we chose $(7, 4)$, $(15, 11)$, and $(31, 26)$ Hamming[1] codes as well as the $(133, 171)$ convolutional code (CC) with code rates $R_\mathrm{c} \in \left\{\frac{1}{2}, \frac{2}{3}, \frac{3}{4}, \frac{5}{6}\right\}$. All codes

[1]Note that we use the code rate of all codes in the plots, so the $(7, 4)$ Hamming code is named $4/7$ Ham(ming).

Parameter	Symbol	Unit	Values
Packet size	n_{data}	B	$8, 64$
Number of evaluated packets	n_{pkt}	—	2700
Relative speed	v	$\mathrm{m\,s^{-1}}$ (Doppler Shift)	$0, 0.75, 1.5, 3, 6$

Table 2: Simulation parameters for coded FSCM transmissions; parameters unchanged from Table 1 have been omitted.

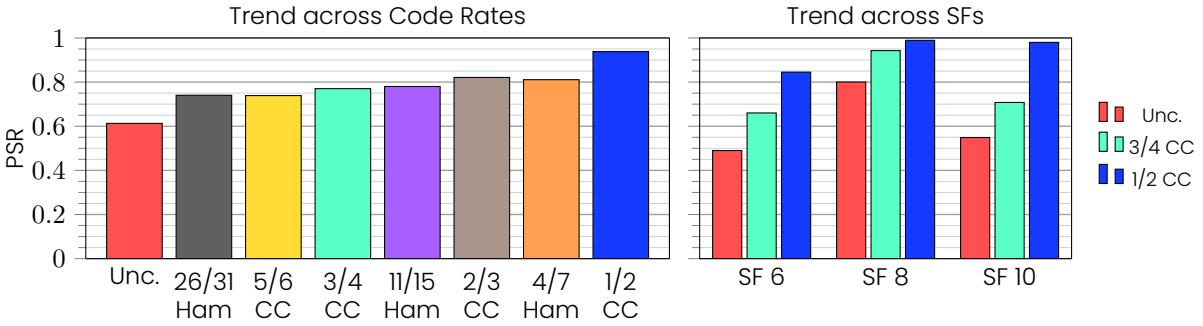

Figure 4: Mean PSR of FSCM transmissions vs. channel codes with block interleaving (left) and spreading factor (right). Results are limited to SNRs ≥ 0 dB.

are combined with block interleaving. We analyze the impact of the codes through PSRs—as an indicator for communication reliability—and data rate. Parameters that were changed from the previous study are summarized in Table 2.

4.1. PACKET SUCCESS RATE

Figure 4 (left plot) shows the mean PSRs (after decoding) for the different codes over all evaluated conditions, in decreasing order of code rate. The PSR increases as the code rate decreases, reflecting the stronger error correction due to added redundancy. The rate-1/2 convolutional code achieves the highest PSR of $93.8\,\%$, improving the uncoded case by approximately $30\,\%$ points. This gain exceeds that of all other evaluated codes by more than $10\,\%$ points. The remaining codes achieve PSRs between $73.9\,\%$ and $82.1\,\%$, with similar code rates yielding comparable results. Notably, the rate-2/3 convolutional code matches the $(7, 4)$ Hamming code in terms of PSR, despite its higher code rate.

When comparing the mean PSR vs. spreading factor, displayed in Fig. 4 (right plot) for uncoded transmissions and convolutional coding with $R_{\text{c}} \in \left\{\frac{3}{4}, \frac{1}{2}\right\}$, the impact of channel coding varies: the strongest gains occur at $\mathrm{SF} = 10$, where the rate-1/2 convolutional code raises the mean PSR to $98\,\%$, which is more than $20\,\%$ points higher than any other evaluated code. At $\mathrm{SF} = 8$, improvements are smaller, and even weaker codes achieve high PSRs, such as $94.3\,\%$ with the rate-3/4 convolutional code, reflecting the balanced resilience of $\mathrm{SF} = 8$ to noise and Doppler shifts observed in the uncoded analysis. At $\mathrm{SF} = 6$, coding still provides clear gains, but its increased susceptibility to multipath effects limits overall reliability, with mean PSRs remaining below $85\,\%$.

4.2. DATA RATE

Beyond error correction capability, the data rate is a key performance aspect of coded FSCM transmissions. The gross data rate of FSCM is the ratio of the number of bits SF and the du-

ration T_{sym} per symbol with $T_{\text{sym}} = 2^{\text{SF}}/\text{BW}$. If channel coding is used, the data rate R_{b} is proportional to the code rate R_{c} and the gross data rate. Relative to SF $= 6$, the data rates for SF $= 8$ and 10 are $33.3\,\%$ and $10.4\,\%$, respectively.

While both the spreading factor and code rate have a significant impact on the data rate of coded FSCM transmissions, the spreading factor is the primary determinant. Therefore, to achieve high data rates, high code rates and, in particular, low spreading factors should be selected. Simultaneously, higher data rates lead to decreased power consumption, as the number of samples per packet is directly proportional to the packet duration. This consideration is particularly relevant for low-power UWAC systems.

4.3. DISCUSSION OF CODING SELECTION FOR SYSTEM INTEGRATION

Stronger coding schemes, such as the rate-1/2 convolutional code, offer superior error correction but introduce substantial redundancy, thereby reducing the data rate. Consequently, optimal channel coding in FSCM-based low-power UWAC systems must balance error correction strength and data efficiency to ensure overall system suitability.

As shown in Sections 4.1 and 4.2, both error correction capability and data rate depend not only on the selected coding scheme, but also on the spreading factor. The spreading factor has the dominant effect on the data rate due to its exponential influence on symbol duration. In terms of communication reliability, however, higher spreading factors improve synchronization by enabling more precise Doppler estimation and achieve higher PSRs in multipath-dominated environments. As demonstrated in Fig. 4, SF $= 6$ provides the lowest reliability with mean PSRs below $85\,\%$, while SF $= 8$ and SF $= 10$ achieve nearly error-free transmission when supported with adequate coding. Between the two, SF $= 8$ offers higher data efficiency and achieves higher PSRs with weaker codings, making it the most suitable choice for FSCM-based low-power UWAC systems.

Beyond the spreading factor, coding effectiveness also varies with parameters such as data length, Doppler shift, and SNR. These variations highlight the need for adaptive coding strategies that respond to scenario-specific constraints. Due to the page limit, we concentrate on mobile scenarios and SF $= 8$. As shown in Fig. 5, convolutional and Hamming codes achieve similar PSRs for similar code rates. In general, the PSR is negatively affected by larger packet size and higher speed. For longer data packets, and particularly in the high-mobility scenario, the code rate has a stronger effect on the PSR.

A closer examination of the convolutional codes in Fig. 5 reveals that for short $(8\,\text{B})$ packets all rates achieve PSRs above $95\,\%$, even under high mobility. Thus, for short messages the rate-5/6 convolutional code and the $(31, 26)$ Hamming code appear to offer the most efficient choice. However, for very small packet sizes, the code and packet structure play a crucial role: For the proposed choices, the Hamming code operates on blocks of 26 data bits, whereas the convolutional coder adds one redundant bit at the beginning of each 5-bit input cycle. For a $7\,\text{B}$ packet, e.g., the coded data has a length of $93\,\text{bit}$ (3 blocks) and $68\,\text{bit}$ (11 cycles plus one input bit) for Hamming and convolutional coding, respectively. For SF $= 8$ in combination with block interleaving, $96\,\text{bit}$ and $72\,\text{bit}$ are transmitted. Therefore, convolutional codes are favorable due to the higher actual data rate at similar PSR.

For longer $(64\,\text{B})$ packets, however, mobility has a greater impact. In low-mobility conditions, codes with $R_{\text{c}} \leq \frac{3}{4}$ enable mean PSRs above $95\,\%$, but only the rate-1/2 convolutional code maintains this reliability in high-mobility scenarios. If packet retransmissions are tolerable, a lower code may be preferable, because the overall bandwidth usage is typically lower; i.e., the expected number of bits to be transmitted for successful packet transmission is lower.

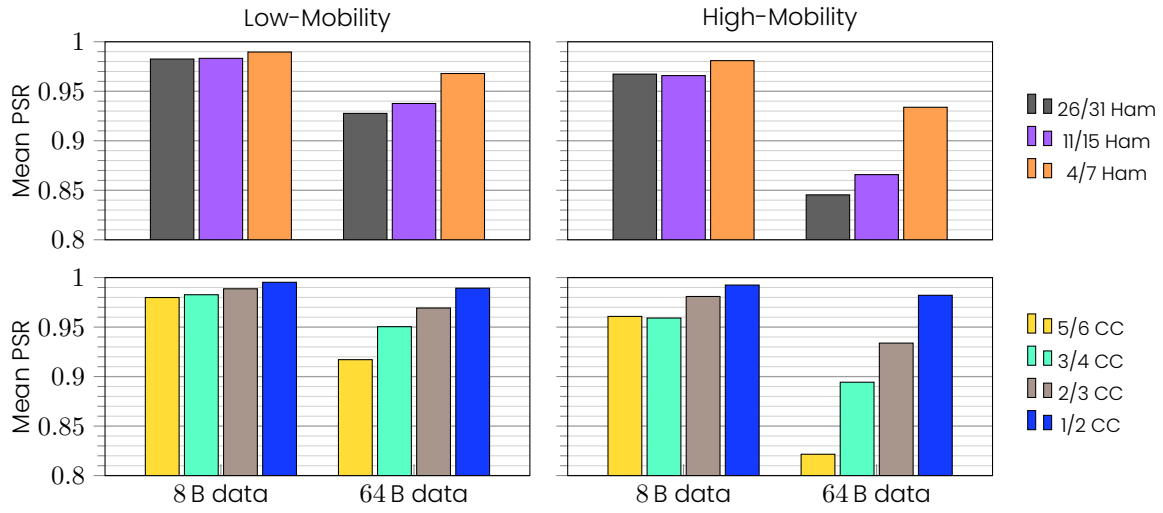

Figure 5: Mean PSRs for different channel codes with block interleaving for $\mathrm{SF} = 8$ *in low-mobility (*$v \in \{0, 0.75\}\,\mathrm{m\,s^{-1}}$*) and high-mobility (*$v \in \{1.5, 3, 6\}\,\mathrm{m\,s^{-1}}$*) scenarios.*

The exact spot of the break-even-point, though, depends on other parameters as, e.g., the length of the packet preamble.

In summary, robust and efficient low-power underwater communication using FSCM requires a joint selection of spreading factor and coding scheme. A spreading factor of $\mathrm{SF} = 8$ combined with the $(133, 171)$ convolutional code and a small set of puncturing patterns, enables a practical, flexible, and adaptive coding strategy. This approach maintains high PSRs across diverse underwater conditions while preserving high data rates.

5. CONCLUSION

We presented our results of a comprehensive simulation study of bit errors and packet success rates for uncoded and coded FSCM transmissions. We identified suitable codes and discussed the influence of several parameters. We found that a spreading factor $\mathrm{SF} = 8$, combined with the rate-adaptable $(133, 171)$ convolutional code and classical block interleaving is recommended for low-power UWAC systems. It achieves a balance between high reliability and data rate across diverse transmission conditions.

REFERENCES

[1] Q. Chen, L. Zhao, Y. Chu, and W. Guo. Research on Multipath Reception and Soft Decision Algorithms for Frequency Shift Chirp Modulation. In *Int. Symposium on Networks, Computers and Communications (ISNCC)*, Shenzhen, China, July 2022. IEEE.

[2] U. Coutaud and B. Tourancheau. Channel Coding for Better QoS in LoRa Networks. In *14th Int. Conf. on Wireless and Mobile Computing, Networking and Communications (WiMob)*, Limassol, Cyprus, Oct. 2018. IEEE.

[3] C. Demeslay, P. Rostaing, and R. Gautier. Simple and Efficient LoRa Receiver Scheme for Multipath Channel. *IEEE Internet of Things Journal (IoT-J)*, 9(17), Sept. 2022.

[4] E. Felemban, F. K. Shaikh, U. M. Qureshi, A. A. Sheikh, and S. B. Qaisar. Underwater Sensor Network Applications: A Comprehensive Survey. *Int. Journal of Distributed Sensor Networks*, 11(11), Nov. 2015.

[5] J. C. Liando, A. Gamage, A. W. Tengourtius, and M. Li. Known and Unknown Facts of LoRa: Experiences from a Large-scale Measurement Study. *ACM Transactions on Sensor Networks*, 15(2), Feb. 2019.

[6] Y. Lou and N. Ahmed. *Underwater Communications and Networks*. Springer Int. Publishing, 2022.

[7] A. Petroni, G. Scarano, R. Cusani, and M. Biagit. Feasibility and Performance Analysis of Underwater Acoustic LoRa Modulation. In *IEEE Int. Conf. on Communications Workshops (ICC Workshops)*, Rome, Italy, May 2023.

[8] J. G. Proakis and M. Salehi. *Digital communications*. McGraw-Hill, Boston, Mass. [u.a.], 5th edition, 2008.

[9] B.-C. Renner, J. Heitmann, and F. Steinmetz. ahoi: Inexpensive, Low-power Communication and Localization for Underwater Sensor Networks and μAUVs. *ACM Transactions on Sensor Networks*, 16(2), Jan. 2020.

[10] M. Rezzouki and G. Ferre. Design and Implementation of Differential Chirp Spread Spectrum System for Underwater Acoustic Communication. In *OCEANS*, Hampton Roads, VA, USA, Oct. 2022. IEEE.

[11] A. Signori, F. Campagnaro, F. Steinmetz, B.-C. Renner, and M. Zorzi. Data Gathering from a Multimodal Dense Underwater Acoustic Sensor Network Deployed in Shallow Fresh Water Scenarios. *Journal of Sensor and Actuator Networks*, 8(4), Nov. 2019.

[12] F. Steinmetz and B.-C. Renner. Taking LoRa for a Dive: CSS for Low-Power Acoustic Underwater Communication. In *6th Underwater Communications and Networking Conf. (UComms)*, Lerici, Italy, Aug. 2022. IEEE.

[13] F. Steinmetz and B.-C. Renner. Doppler Shift and SFO Robust Synchronization for LoRa-Like Acoustic Underwater Communication. *IEEE Access*, 11, 2023.

[14] F. Steinmetz and C. Renner. Practical Evaluation of Differential Frequency Shift Chirp Modulation for Acoustic Underwater Communication. In *Proceedings of the 17th Int. Conf. on Underwater Networks & Systems*, WUWNet 2023, New York, NY, USA, Nov. 2023. ACM.

[15] M. Stojanovic and J. Preisig. Underwater acoustic communication channels: Propagation models and statistical characterization. *IEEE Communications Magazine*, 47(1), Jan. 2009.

[16] J. Tapparel, O. Afisiadis, P. Mayoraz, A. Balatsoukas-Stimming, and A. Burg. An Open-Source LoRa Physical Layer Prototype on GNU Radio. In *IEEE 21st Int. Workshop on Signal Processing Advances in Wireless Communications (SPAWC)*, Atlanta, GA, USA, May 2020.

[17] P. A. van Walree, F.-X. Socheleau, R. Otnes, and T. Jenserud. The Watermark Benchmark for Underwater Acoustic Modulation Schemes. *IEEE Journal of Oceanic Engineering (JOE)*, 42(4):1007–1018, Oct. 2017.

[18] L. Vangelista. Frequency Shift Chirp Modulation: The LoRa Modulation. *IEEE Signal Processing Letters*, 24(12), Dec. 2017.

[19] M. Xhonneux, O. Afisiadis, D. Bol, and J. Louveaux. A Low-Complexity LoRa Synchronization Algorithm Robust to Sampling Time Offsets. *IEEE Internet of Things Journal (IoT-J)*, 9(5), Mar. 2022.

[20] K. Yang and W. Du. A Low-Density Parity-Check Coding Scheme for LoRa Networking. *ACM Transactions on Sensor Networks*, 20(4), July 2024.

[21] T. Ye, B. Qin, W. Cheng, Z. Peng, S. Song, and J. Cui. Recursive Distortion Recovery by Leveraging Interference in CSS-based UWAC Systems. In *ACM Int. Conf. on Underwater Networks & Systems (WUWNet)*, Šibenik, Croatia, Oct. 2024.